

Project No: 603502

**DACCIWA**

"Dynamics-aerosol-chemistry-cloud interactions in West Africa"

**Deliverable**

**D6.2 Rainfall classification**

**Due date of deliverable:** 30/11/2017  
**Completion date of deliverable:** 28/11/2017

**Start date of DACCIWA project:** 1<sup>st</sup> December 2013    **Project duration:** 60 months

**Version:** [V1.0]  
**File name:** [D.06.2\_rainfallclassification\_v1.0.pdf]

**Work Package Number:** 6  
**Task Number:** 2

**Responsible partner for deliverable:** KNUST  
**Contributing partners:** KIT, UPS

**Project coordinator name:** Prof. Dr. Peter Knippertz  
**Project coordinator organisation name:** Karlsruher Institut für Technologie

The DACCIWA Project is funded by the European Union's Seventh Framework Programme for research, technological development and demonstration under grant agreement no 603502.

Dissemination level		
<b>PU</b>	Public	<b>x</b>
<b>PP</b>	Restricted to other programme participants (including the Commission Services)	
<b>RE</b>	Restricted to a group specified by the consortium (including the Commission Services)	
<b>CO</b>	Confidential, only for members of the consortium (including the Commission Services)	

Nature of Deliverable		
<b>R</b>	Report	
<b>P</b>	Prototype	
<b>D</b>	Demonstrator	
<b>O</b>	Other	<b>x</b>

### Copyright

This Document has been created within the FP7 project DACCIWA. The utilization and release of this document is subject to the conditions of the contract within the 7<sup>th</sup> EU Framework Programme. Project reference is FP7-ENV-2013-603502.

**DOCUMENT INFO****Authors**

Author	Beneficiary Short Name	E-Mail
Leonard Amekudzi	KNUST	<a href="mailto:leonard.amekudzi@gmail.com">leonard.amekudzi@gmail.com</a>
Winifred Ayinpogbilla Atiah	KNUST	<a href="mailto:winifred.a.atiah@aims-senegal.org">winifred.a.atiah@aims-senegal.org</a>
Andreas H. Fink	KIT	<a href="mailto:andreas.fink@kit.edu">andreas.fink@kit.edu</a>
Marlon Maranan	KIT	<a href="mailto:marlon.maranan@kit.edu">marlon.maranan@kit.edu</a>
Jean-Pierre Chaboureau	UPS	<a href="mailto:jean-pierre.chaboureau@aero.obs-mip.fr">jean-pierre.chaboureau@aero.obs-mip.fr</a>
Irene Reinares Martinez	UPS	<a href="mailto:irene.reinares@aero.obs-mip.fr">irene.reinares@aero.obs-mip.fr</a>

**Changes with respect to the DoW**

Issue	Comments

**Dissemination and uptake**

Target group addressed	Project internal / external
Scientific community	Internal and external

**Document Control**

Document version #	Date	Changes Made/Comments
0.1	15.11.2017	First version for approval by the GA
1.0	28.11.2017	Final version approved by the GA

## Table of Contents

1	Introduction .....	5
2	Satellite-based Identification and Climatology of Rainfall Types .....	5
2.1	Data and Methods .....	5
2.1.1	Definition of Rainfall Types .....	5
2.1.2	Combination with Reanalysis and Satellite Infrared Data .....	6
2.2	Number and Rainfall Contribution of Rainfall Types .....	6
2.3	Properties of Rainfall Types .....	7
2.4	Environmental conditions .....	8
3	A modelling case study from the 2006 AMMA campaign.....	9
3.1	Model and data .....	9
3.2	Precipitation and MCSs for explicit versus parameterized convection over northern Africa 10	
3.3	Radiative effect of dust on mesoscale convective systems .....	11
4	Rain gauge-based rainfall analysis over the Ashanti Region of Ghana during the 2016 and 2017 rainfall seasons .....	11
4.1	Rain gauge and study area .....	11
4.2	Properties of rainfall systems detected by the DOG network.....	13
4.3	Summary .....	15
5	References:.....	16

# 1 Introduction

West Africa exhibits one of the most variable climates on earth, where substantial fluctuations of rainfall on annual to decadal timescales have long been identified. The high socio-economic relevance of rainfall in this region was dramatically exposed during the abnormally dry period that commenced in the late 1960s and peaked during strong drought years in the early 1970s and 1980s. To this day, rainfall is the most influencing factor for farming, energy and fresh water supply in the West African countries whose economies predominantly rely on agriculture. In contrast, occasional floodings in the past due to long-lasting, heavy rainfall have led to a significant number of casualties and negative impacts on the infrastructure in densely populated regions and cities. The occurrence of such events on the extreme end of the rainfall spectrum has given rise to numerous studies on rainfall variability over West Africa where the bulk has focused on the often drought-stricken Sahelian region. In general, the interannual variability has been suggested to be closely related to the occurrence frequency of different types of rainfall systems, which, in turn, develop under different environmental conditions. These rainfall types range from shallow, “warm-rain”-producing cloud elements to large organized, self-sustaining convective systems termed “Mesoscale Convective Systems (MCSs)”. While it is now commonly known that the latter account for the vast majority of rainfall in the Sahel, there is a lack of robust rainfall type statistics for the wetter and more populous region of Southern West Africa (SWA) lying to the south of the Sahel. Furthermore, the (thermo-) dynamical environments that influence the development of the various rainfall types over SWA are still poorly understood.

The present report provides an extensive analysis of the relevant rainfall types for SWA, their contribution to total rainfall and the environmental controls under which they occur. These points are presented from three different perspectives: First, the rainfall systems were investigated based on various satellite products which are further combined with reanalysis data of the atmospheric fields. Secondly, an assessment of rainfall types is given from the viewpoint of a state-of-the-art numerical model. Finally, recordings from the dense network of high-resolution raingauges around Kumasi (Ghana), which was established in the framework of the DACCIWA project, were exploited to obtain “ground-truth” rainfall information at a fixed location close to the Guinea coast.

## 2 Satellite-based Identification and Climatology of Rainfall Types

### 2.1 Data and Methods

#### 2.1.1 Definition of Rainfall Types

As it provides one of the most accurate space-borne rainfall estimates for the tropical belt, rainfall systems were identified using three-dimensional rainfall reflectivity signals from the Tropical Rainfall Measuring Mission Precipitation Radar (TRMM-PR) for its operational period 1998-2013. Subsequently, rainfall types were stratified into seven classes based on the intensity and the horizontal and vertical structure of the reflectivity volumes, following an extended version of the method introduced in Houze et al. (2007, 2015). These rainfall types exhibit different degrees of convective organization and range from isolated and shallow elements on the weak end to cloud systems with an extensive convective and stratiform rainfall region on the intense end of the convective spectrum, typically representing MCSs. In the following, for the sake of simplicity, we refer to two groups, namely “Diurnal Convection” and “MCS” (for details, see schematic in Fig. 1).

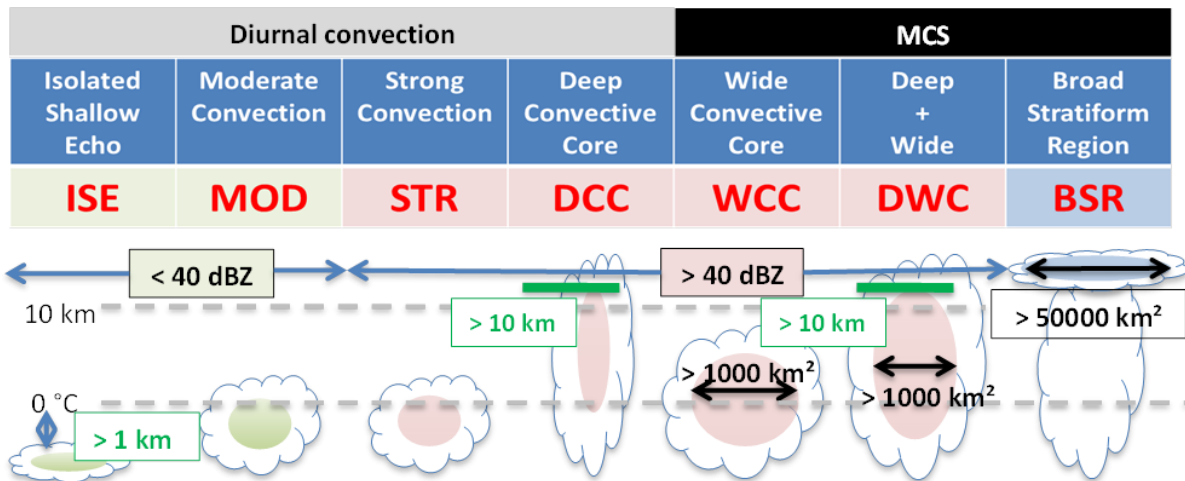


**Figure 1:** Extended version of the rainfall classification after Houze et al. (2007, 2015). A radar reflectivity threshold of 40 dBZ is used to distinguish between weaker (green category) and stronger systems (red category). Further distinctions are based on height and area criteria (green and black numbers, respectively) of the 40 dBZ reflectivity volumes. The blue category, BSR, is identified based on a contiguous stratiform rainfall area of 50,000 km<sup>2</sup>.

**2.1.2 Combination with Reanalysis and Satellite Infrared Data**

One of the drawbacks using the high-resolution TRMM-PR is the introduction of sampling errors since only four to six overpasses over SWA per day occurred. Thus, TRMM-PR provides random “snapshots” of rainfall and no continuous observation. Therefore, TRMM-PR information are combined with spatio-temporally continuous infrared cloud information from the geostationary Meteosat Spinning Enhanced Visible and Infrared Imager (SEVIRI) to track the lifecycle of rainfall systems and to mitigate the sampling error. This is performed for the period 2004-2013 since SEVIRI was not active before 2004. In a further step, reanalysis data of the atmospheric fields from the European Centre for Medium-Range Weather Forecast (ECMWF) are used to compile the typical environmental controls for the various rainfall types.

**2.2 Number and Rainfall Contribution of Rainfall Types**

In order to highlight regional differences of the composition of rainfall, a subdivision of the SWA region was performed (Fig. 2a). This includes the 100 km wide “Coast” region as the most southern region (blue), the subsequent “Inland” region to the north up to 9°N (orange) which roughly comprises the forested zone of SWA, and finally the drier “Sudan” region (9°N-12°N, red) which is widely considered as the transition region to the Sahel in the north. In Fig. 2b, both the fractional number of rainfall events (lines) and the fractional rainfall contribution of the rainfall types (bars) are shown with respect to the aforementioned subregions. Irrespective of the subregion, the rainfall types belonging to the MCS group are altogether the main contributor to total rainfall in SWA although they are strongly outnumbered by less intense diurnal rainfall systems. However, a latitudinal dependency is found where the rainfall contribution of MCSs decreases from 71% in the Sudan region to 56% at the coast. Accordingly, the importance of diurnal convection to total rainfall increases southward. The differences among the subregions are further highlighted by the latitudinal dependency of the number of isolated, shallow echoes (ISE) which is highest at the coast. These pure “warm-rain” elements are typical phenomena over the ocean. It can be concluded that due to the immediate vicinity to the ocean, a more maritime environment at the coast prevails that promotes the development of these shallow rainfall type. However, contrary to the number, their rainfall contribution is low at the coast (2%) and negligible in the other two subregions.

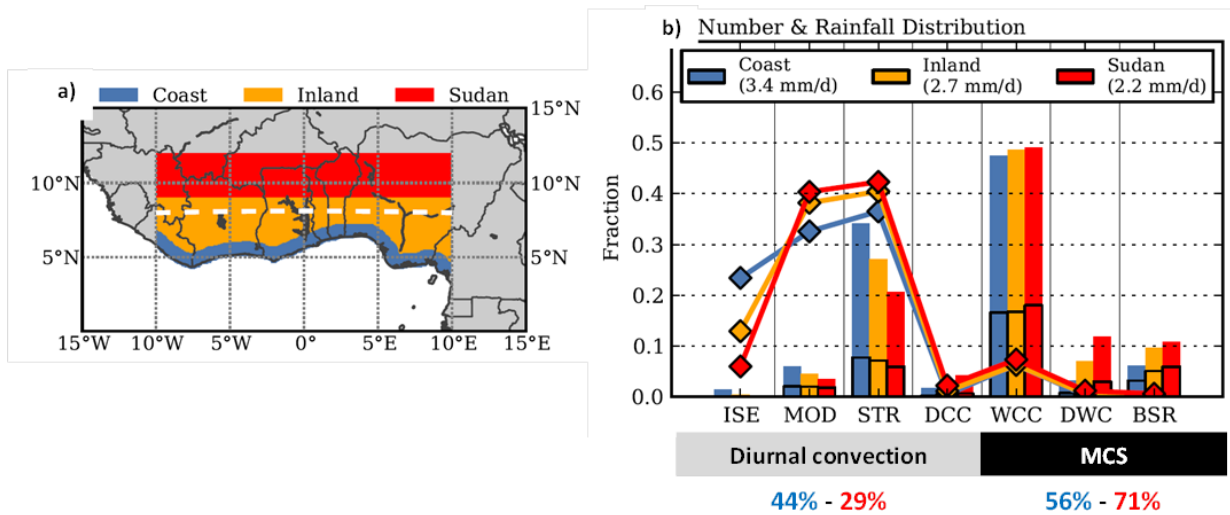


**Figure 2:** (a) Definition of the SWA subregions “Coast” (blue) as a 100 km-wide coastal strip, “Inland” (orange) extending north until 9°N, and “Sudan” (red) from 9°N to 12°N. Each subregion is zonally bounded at 10°W and 10°E, respectively. (b) Fractional number (lines) and rainfall contribution (bars) of each rainfall class in each subregion defined in (a). Black-framed bars denote the contribution from stratiform rain. The rainfall rates in the legend indicate the region-averaged daily accumulated rainfall in each region.

### 2.3 Properties of Rainfall Types

For the period 2004-2013 and the SWA region, a large ensemble of cold clouds in the SEVIRI imagery were tracked in space and time to obtain information about their lifetime and translation velocity. The number distribution with respect to these two quantities is presented in Fig. 3a as a two-dimensional histogram. In general, the number of convective systems decreases with longer lifetimes, i.e. short-lived diurnal convection (The groups C1 and C3 in Fig. 3a) dominates the sample. The relationship to the translation velocity is more complex. While these short-lived systems exhibit a wide range of velocities up to 20 m/s, long-lived systems (C2 and C4), which typically represent MCSs, tend to occur only in a specific window between 5 m/s and 15 m/s.

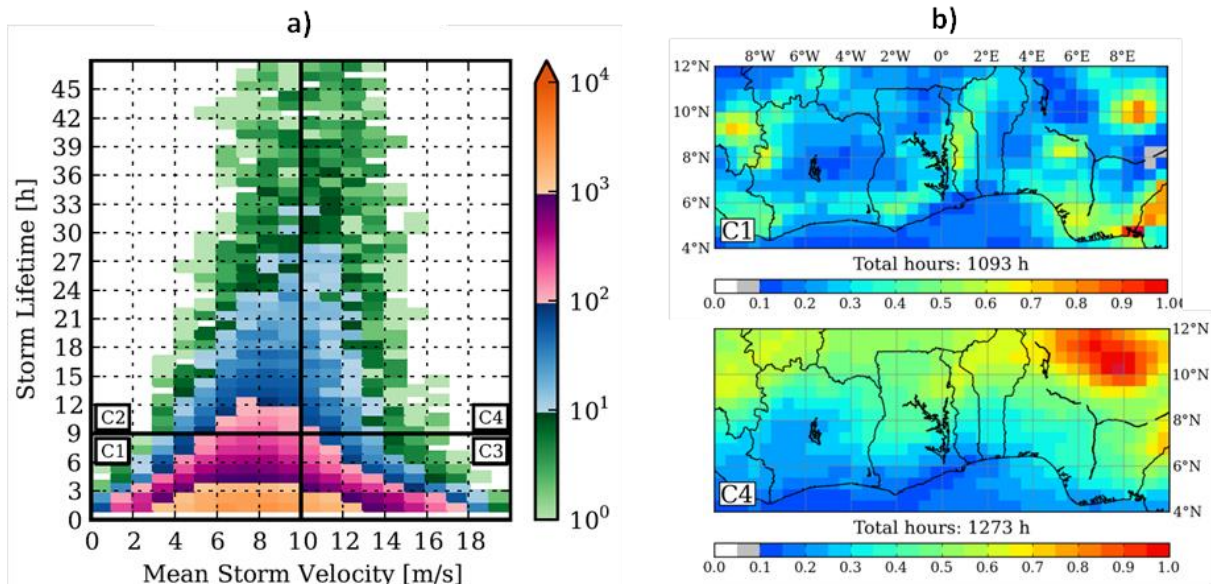


**Figure 3:** (a) Two-dimensional number distribution with respect to lifetime and velocity of tracked cloud systems based on Meteosat IR data. Short and long lifetime is separated by a lifetime threshold of 9h, slow and fast storm propagation by a velocity of 10 m/s, respectively. The subsequent C1-to-C4 categorization is taken from Lafore et al. (2017). (b) Normalized “activity map” for the C1 and C4 category based on their hours of overpass. A value of 1 denotes the maximum overpass hours indicated above the respective colorbars.

The groups C1 and C4 are convective systems on the opposite ends of the lifetime and velocity spectra (short-lived+slow and long-lived+fast, respectively) and are each most active in different areas (Fig. 3b). The activity of C1 systems (Fig. 3b, upper panel) is mostly confined to orographic features, but they are also more likely to develop along the coast. The latter reflects the relevance of the land-sea-breeze circulation to the occurrence of C1. C4 systems predominantly occur in the northern regions of SWA and are less likely to be found towards the coastal regions. This latitudinal dependence of MCS activity was already visible in the previous section.

In Table 1, the TRMM-PR-based rainfall types are assigned to these C-groups. Again, obvious differences are evident for C1 and C4. MCS types identified through TRMM-PR are predominantly long-lived systems, whereas, as expected, diurnal convection identified through TRMM-PR are in fact short-lived. The implication of this finding is that the rainfall contribution of MCSs presented in Fig. 2b should rather be regarded as a lower estimate since the long lifetime of MCSs was not accounted for in this statistics.

**Table 1:** Assignment of TRMM-based rainfall classes (left column) to IR-based classification (top row) and the respective fractional distribution. The distribution of ISEs is unknown as warm precipitating clouds were not tracked.

	C1	C2	C3	C4
ISE	?	?	?	?
MOD	33%	36%	8%	23%
STR	43%	24%	14%	19%
DCC	40%	29%	11%	20%
WCC	24%	37%	8%	31%
DWC	13%	35%	3%	49%
BSR	0%	31%	0%	69%

## 2.4 Environmental conditions

Fig. 4 presents composited time-height diagrams in a 96-hour window around the time of the rainfall event (denoted as a black line) for selected rainfall types, thus showing the environmental conditions before and after. In general, rainfall types over SWA occur in conjunction with anomalies in relative vorticity (shaded in Fig. 4a) at midlevels which alter the horizontal wind field (denoted as anomaly vectors) and thus the magnitude of low-level wind shear (gray line). Sufficiently strong low-level wind shear is known to have a positive impact on the convective organization of rainfall systems. Therefore, depending on the configuration of these vorticity anomalies, different rainfall types are promoted. Diurnal rainfall types typically develop in a regime of anomalous deep westerlies (e.g. ISE case) with suppressed wind shear. In contrast, MCS types tend to occur under the influence of a dipole configuration with a preceding anticyclonic and a succeeding cyclonic disturbance, where wind shear is enhanced. This particular dipole structure is commonly found during the passage of African Easterly Waves (AEW). Although the relationship between AEWs and the occurrence frequency of MCSs is yet not fully understood, the present results emphasize the relevance of such wave disturbances on the growth of convective systems.

Environmental conditions at the surface exhibit certain coherence among the rainfall types with respect to low-level convergence (shaded in Fig. 4b). Prior to the rainfall event, convergent flow prevails at low-levels together with an increase in low-level moisture (black contours). This process

is most pronounced for the MCS types. Moisture convergence typically reduces the convective inhibition (CIN) but increases the convective available potential energy (CAPE), contributing to the development and/or establishment of convective systems. However, the exact controls that lead to moisture convergence over SWA are poorly understood. Future investigations of rainfall cases with DACCIWA field campaign data may aid to shed more light on this.

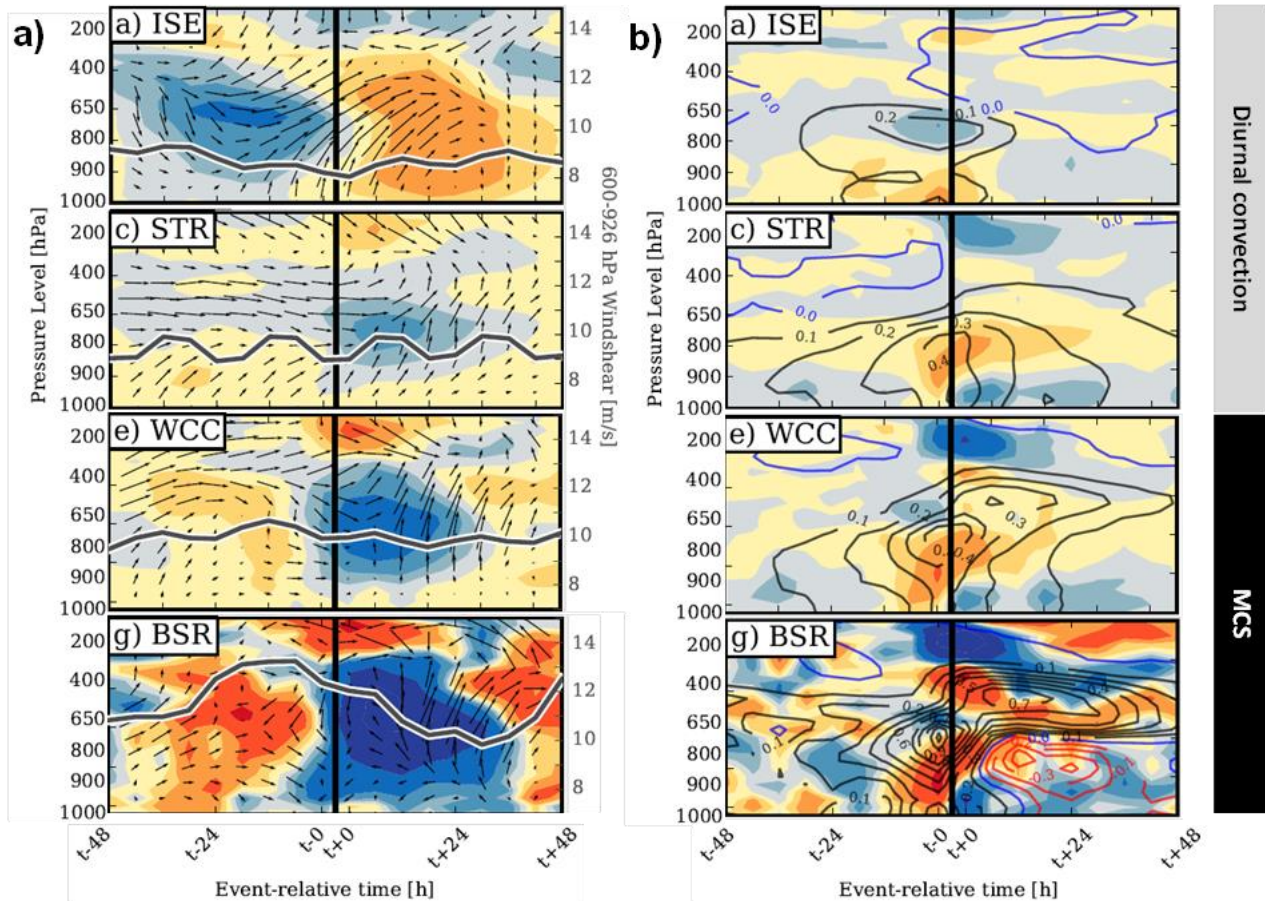


**Figure 4:** (a) ERA-Interim-based composited time-height diagrams in a 48 hours before and after the rainfall event (vertical black line) with respect to the anomaly of relative vorticity (shaded), the anomaly of horizontal wind (vectors). The gray lines indicate the magnitude of the 600-925 hPa wind shear. (b) As in (a), only for the anomaly of convergence (shaded) and the anomaly of specific humidity (contours). Red contours denote a negative anomaly, the blue contour indicate the zero line.

### 3 A modelling case study from the 2006 AMMA campaign

The case study of 9-14 June 2006 examined here is a well-documented episode of dust emission and transport, and MCSs propagation in West Africa (Flamant et al., 2009). It was chosen to investigate the mechanisms controlling precipitation in northern Africa. Specifically, the underlying processes leading to the organization of MCSs have been addressed. On one hand, the impact of the resolution and the representation of convection on the characteristics of the MCSs is examined. On the other hand, the radiative effect of dust on the MCSs is explored.

#### 3.1 Model and data

Three simulations were run with the non-hydrostatic mesoscale atmospheric Méso-NH model (Lafore et al. 1998), over a domain of  $3840 \times 7680 \text{ km}^2$  covering northern Africa. One simulation was run with a 20-km horizontal grid and parameterized convection, a set up typical of regional

climate models. The two others were run with a 2.5-km horizontal grid that permits the convection to be represented explicitly. They differ in the representation of dust, one using a dust prognostic scheme to allow online interaction with dust and the other without any dust radiative effect.

A common method is applied to the observations and to three simulations. Cloud systems were defined in terms of brightness temperature (BT) at 10.8  $\mu\text{m}$  and 3-hourly accumulated precipitation was associated with them. The observation data sets are the Meteosat Second Generation (MSG) BT and the TRMM 3B42 product. From the model outputs, synthetic MSG BTs were calculated. The precipitating systems are identified as cloud objects and classified as deep convective clouds (DCCs) or other clouds according to their infrared signature. Large DCCs (named MCSs hereafter) are tracked, characterized in terms of precipitation and thermodynamic profiles, and analyzed in southern West Africa (SWA), Central Africa (CAF) and Ethiopia (ETH).

### 3.2 Precipitation and MCSs for explicit versus parameterized convection over northern Africa

Precipitation is mostly observed along 0-15°N, with 71% of the total precipitation produced by all DCCs and 55% by long-lived MCSs (Fig. 5). It shows a marked diurnal cycle with a peak in the evening, mainly due to long-lived MCSs, which are characterized by an increase in size, zonal speed and duration from east to west, with the largest, fastest and longest-lived found over SWA. This is due to an enhanced African Easterly Jet (AEJ) and monsoon flow leading to stronger shear and greater conditional instability. The simulation with parameterized convection fails to distribute precipitation correctly. The convection-permitting simulation captures most of the observed precipitation features, but lacks the increase in organization of the long-lived MCSs over SWA. The too strong moisture in a too zonal AEJ flow suggests that the long-lived MCSs in SWA are poorly located with respect to African Easterly Waves. The convection-permitting model improves the representation of precipitation but without fully resolving the long-lived MCSs (Reinares Martínez and Chaboureau, 2017a).

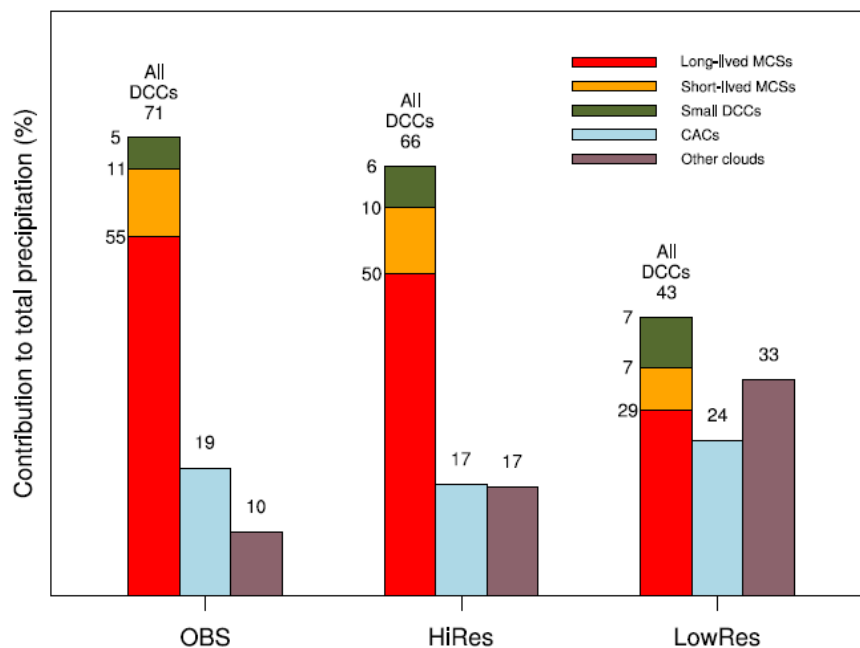


**Figure 5:** Contribution of all the DCCs (long- and short-lived MCSs and small DCCs), CACs (cirrus anvil clouds) and other clouds to total precipitation over the whole domain for the observations and the simulations. HiRes is the convection-permitting simulation with 2.5-km grid spacing and HiNod is the one with parameterized convection and 20-km grid spacing.

### 3.3 Radiative effect of dust on mesoscale convective systems

Dust outbreaks were reported in the Bodélé Depression in Chad and in Sudan during the 9-14 June 2006 period (Flamant et al., 2009), which are simulated at the right locations. The dust radiative effect on the atmosphere is then analyzed, by comparing the two convection-permitting simulations, with and without dust-radiation interaction. The direct effects are a mid-level warming and a near-surface cooling mainly in the western parts of northern Africa, that tend to stabilize the lower atmosphere. One semi-direct effect is a decrease in precipitation. This rainfall decrease is explained by a too low number of long-lived MCSs which, once being generated, are very long-living and more efficient in terms of precipitation production (Fig. 6). The diminution in the number of long-lived MCSs is due to the stabilization of the atmosphere inhibiting the triggering of convection (Reinares Martínez and Chaboureau, 2017b).

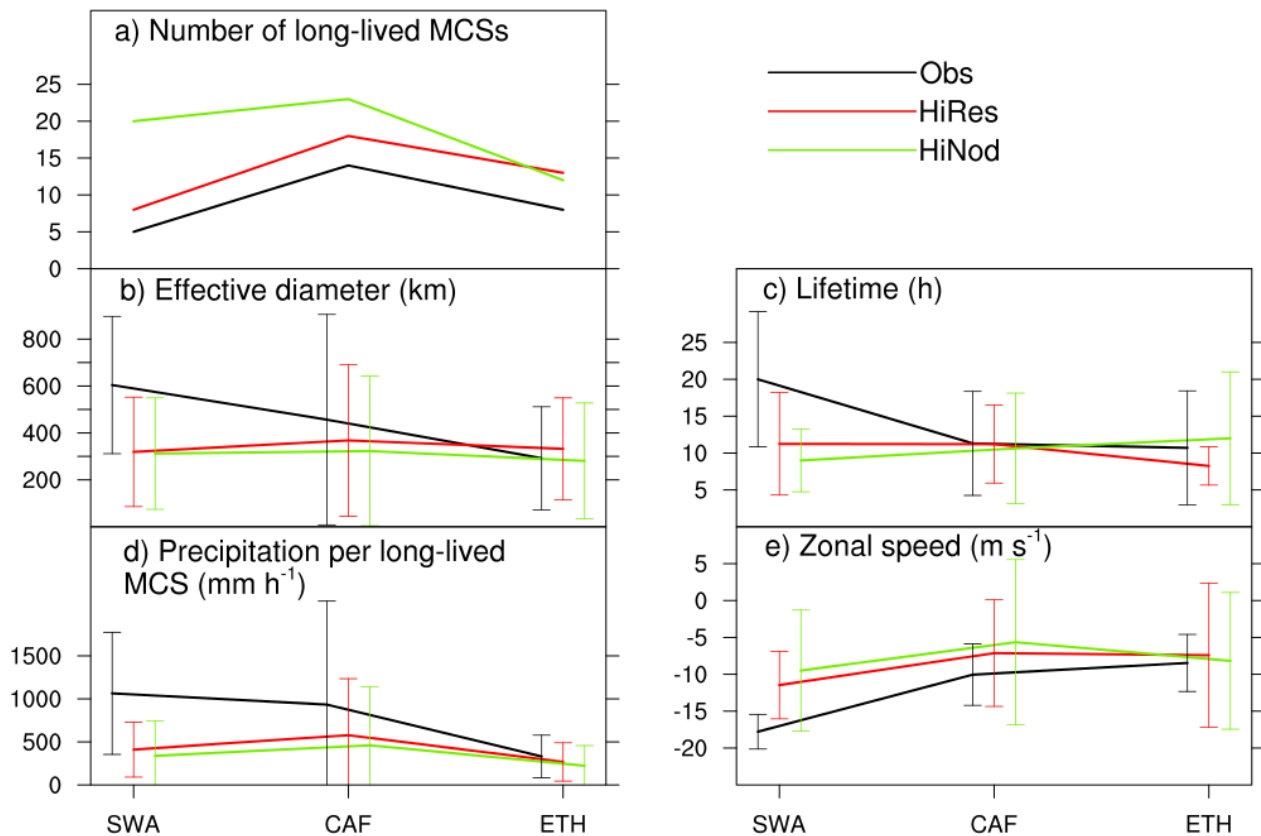


**Figure 6:** Characteristics of long-lived MCSs by sub-region (SWA, CAF, ETH) for the observations and the simulations: (a) number of long-lived MCSs, (b) effective diameter, (c) lifetime, (d) precipitation per long-lived MCS and (e) zonal speed. In (b)-(e) the solid lines represent the mean values and the error bars the standard deviation (HiRes is the simulation with dust-radiation interaction, HiNod is the one without interaction).

## 4 Rain gauge-based rainfall analysis over the Ashanti Region of Ghana during the 2016 and 2017 rainfall seasons

### 4.1 Rain gauge and study area

Seventeen DACCIWA optical rain gauges (DOGs) are currently deployed at different locations over the Ashanti region of Ghana (ARG) within a radius of approximately 70 km around Kumasi (Fig. 7). The installation of the rain gauge network was completed in December 2015. They were strategically mounted at convenient locations, especially on school grounds and already existing enclosures of weather stations operated by the Ghana Meteorological Agency (GMet). Thus, a

high standard of security is guaranteed. The upcoming analysis is based on data from January 2016 to September 2017. Summarized information on the various optical rain gauge stations can be found in Table 2.

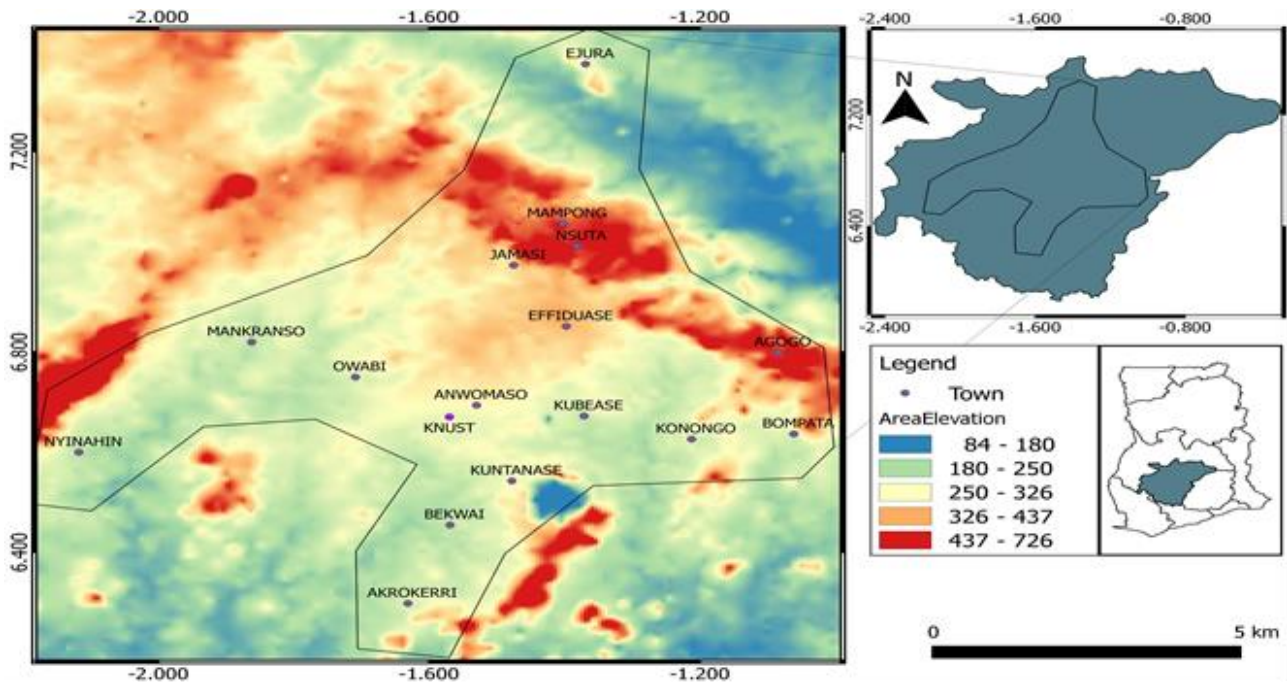


**Figure 7:** Locations of the seventeen DOGs over the Ashanti Region of Ghana. The stations “KNUST” and “Anwomaso” are at the eastern end of the city Kumasi.

**Table 2:** Meta information about the DOG stations. The numbering of the rain gauges are not continuous since three of them (RG03, RG05, RG12) are used as spare elements.

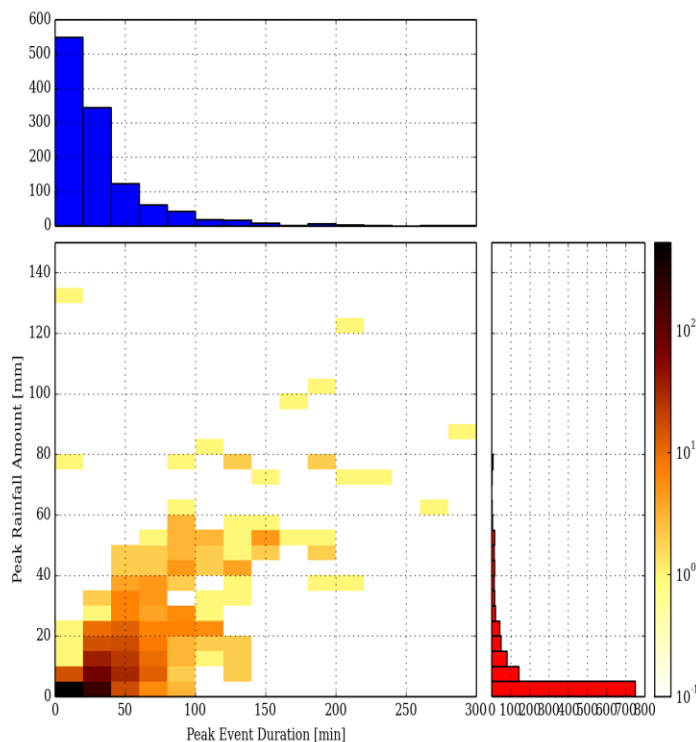
Station Name	Rain Gauge Name	Longitude [W]	Latitude [N]	Elevation [m]
Mampong	RG01	1.24	7.03	439
KNUST	RG02	1.34	6.41	282
Anwomaso	RG04	1.31	6.41	288
Ejura	RG06	1.23	7.22	228
Jamasi	RG07	1.28	6.58	316
Effiduase	RG08	1.24	6.51	368
Akrokeri	RG09	1.39	6.18	259
Bekwai	RG10	1.34	6.27	241
Nyinahin	RG11	2.07	6.35	196
Owabi	RG13	1.42	6.45	237
Kuntanase	RG14	1.29	6.32	301
Nsuta	RG15	1.24	7.00	465
Bompata	RG16	1.03	6.38	236
Konongo	RG17	1.14	6.37	255
Kubease	RG18	1.22	6.40	239
Agogo	RG19	1.04	6.48	417
Mankranso	RG20	1.52	6.80	243

The sensor of the DOG operates on the principle that raindrops, which are formed at the end of the orifice and subsequently fall through the device, are counted. The rainfall amount is then estimated with the assumption that a rain drop is equivalent to 0.01 mm. Rainfall from these optical gauges is provided on a minutely basis.

## 4.2 Properties of rainfall systems detected by the DOG network

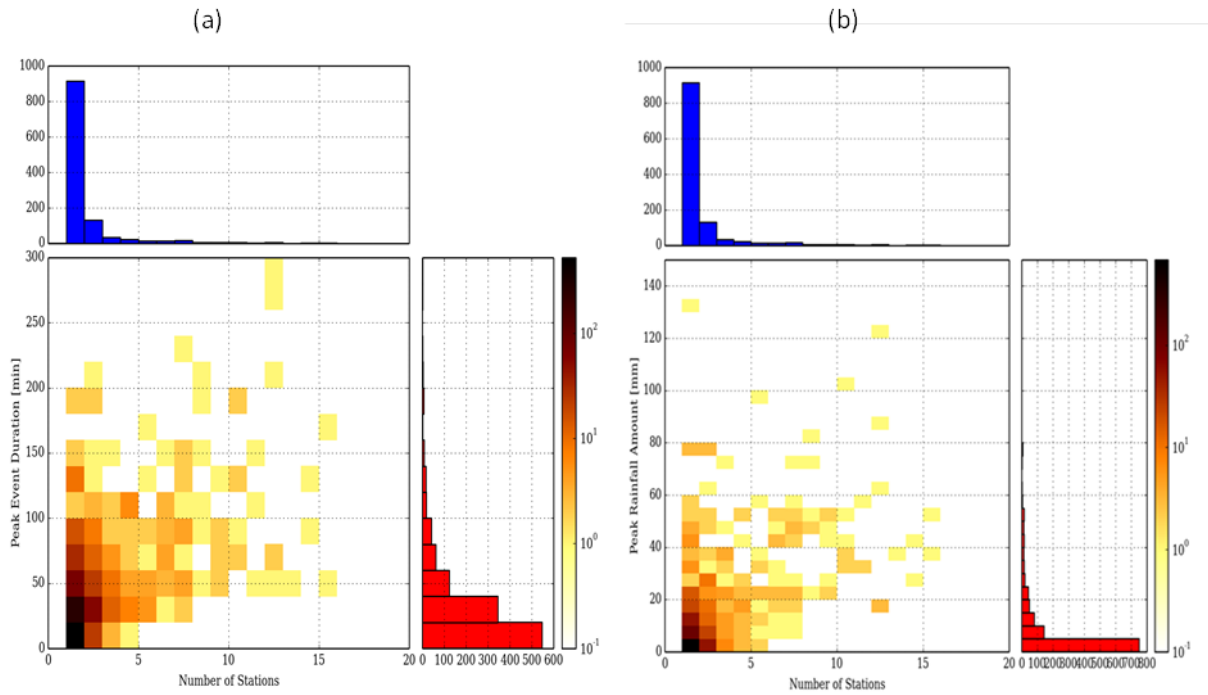
In a first step, distinct rainfall events are identified using a correlation-regression approach introduced in Upton (2001). Rainfall profiles in the DOGs are cross-correlated and eventually assigned to the same rainfall event if they match specific statistical criteria. Thus, the number of stations hit by one single rainfall event can be an indication of the size of a rainfall system. Having defined the events, further properties such as the velocity of the rainfall systems as well as the peak rainfall totals can be derived.

Fig. 8 shows the duration of the rainfall system against the peak rainfall amount. It is conclusive from this figure that the high integrated rainfall amounts generally exhibit a certain degree of correlation with the duration of the event. However, it shows a large spread.



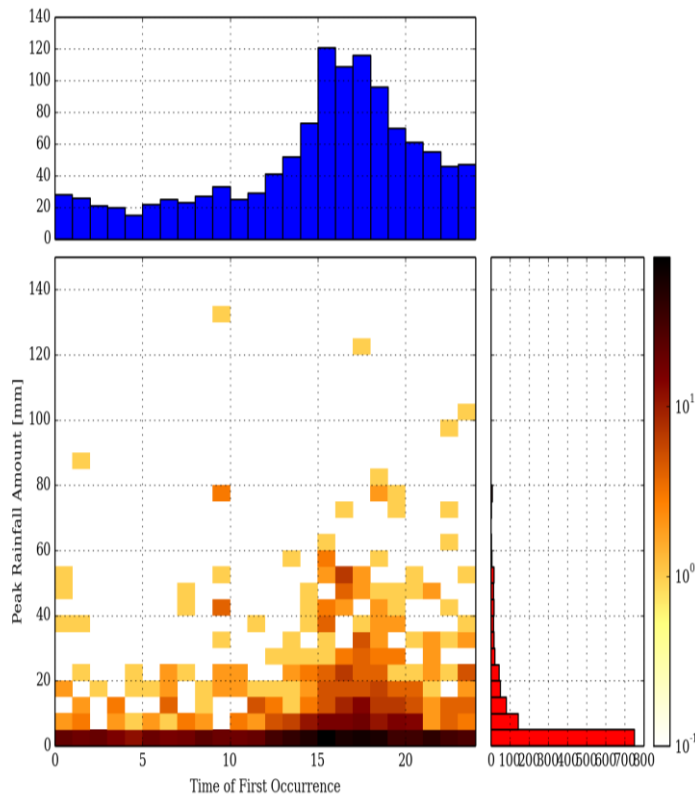
**Figure 8:** 2D-histogram of rainfall events with respect to the peak event duration [min] and the peak rainfall amount [mm]. The histograms at the top and to the right show the event numbers of the columns and rows, respectively.

In Fig. 9, the number of stations is compared against (a) the event duration and (b) the rainfall amount. It is observed that manifold of the rainfall events over the area were influenced by small, short-lived rainfall systems. Overall, the distribution indicates that the number of stations reporting rain (roughly size of the systems) is neither indicator for the duration of an event nor for the peak rainfall amount as the distributions are quite broad. This thereby highlights the variable nature of the rainfall in the ARG.



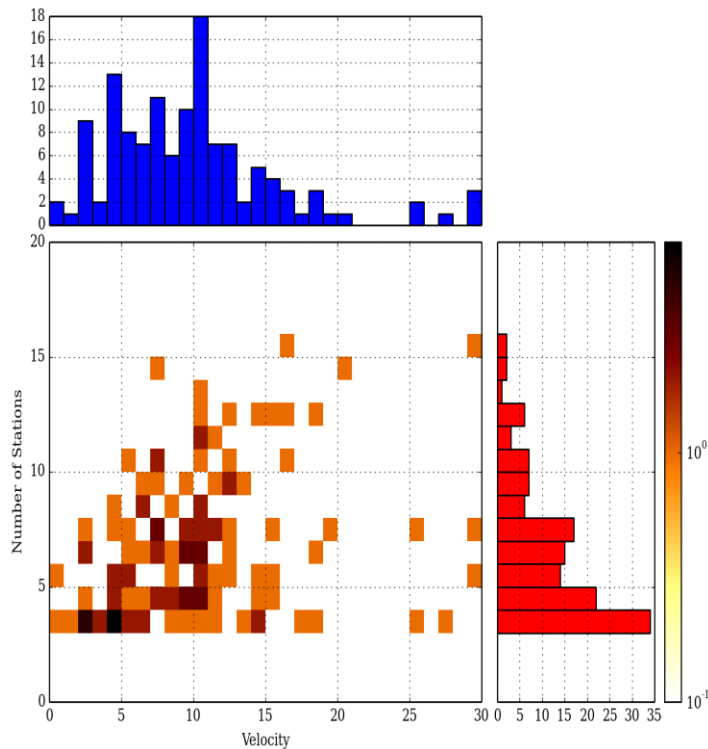
**Figure 9:** As Fig. 8, but with respect to the number of stations and (a) the peak event duration and (b) the peak rainfall amount.

Fig. 10 on the other hand shows the diurnal cycle of the occurrence of rainfall systems with respect to the peak rainfall amount. The distribution is generally dominated by the diurnal cycle of low-intense rainfall events. Most of them occurred between 15:00-20:00 UTC and clearly signify the preference of local convection to develop in the afternoon. High-intense rainfall is also concentrated during this time of the day. However, some these signals are also visible during the early night and late morning and may indicate westward-moving organized convection, like MCSs, that travelled overnight from the eastern regions of West Africa.



**Figure 10:** As Fig. 8, but with respect to the Time of Occurrence (UTC) and the peak rainfall amount.

In Fig. 11, the storm velocity is compared against the number of affected stations. Note that the calculation of the velocity was performed only for events that were recorded by at least three stations. Therefore, single-stations events, which dominate the sample, are excluded here. There is a certain tendency that the number of stations increases with velocity. This suggests that larger, organized convective systems are travelling with a higher velocity. For SWA, the convective systems predominantly exhibit values between 5 m/s and 10 m/s, but can reach velocities up to 20 m/s as well.



**Figure 11:** As Fig. 8, but with respect to the storm velocity and the number of stations

### 4.3 Summary

The rainfall over the ARG has been assessed using minutely rainfall data from the DOGs for the period January 2016 to September 2017. It can be concluded that rainfall is generally dominated by the diurnal cycle of single-station (small) rainfall events. These are suggested to be low-intense, warm-rain producing clouds that most satellites are unable to resolve. Therefore, further studies on their dynamics and the environmental controls are necessary.

## 5 References:

- Houze, Robert A., Darren C. Wilton, and Bradley F. Smull. "Monsoon convection in the Himalayan region as seen by the TRMM Precipitation Radar." *Quarterly Journal of the Royal Meteorological Society* 133.627 (2007): 1389-1411.
- Houze, Robert A., et al. "The variable nature of convection in the tropics and subtropics: A legacy of 16 years of the Tropical Rainfall Measuring Mission satellite." *Reviews of Geophysics* 53.3 (2015): 994-1021.
- Nicholson, Sharon E. "The West African Sahel: A review of recent studies on the rainfall regime and its interannual variability." *ISRN Meteorology 2013* (2013).
- Fink, Andreas H., and Andreas Reiner. "Spatiotemporal variability of the relation between African easterly waves and West African squall lines in 1998 and 1999." *Journal of Geophysical Research: Atmospheres* 108.D11 (2003).
- Le Barbé, Luc, Thierry Lebel, and Dominique Tapsoba. "Rainfall variability in West Africa during the years 1950–90." *Journal of climate* 15.2 (2002): 187-202.
- Kawanishi, Toneo, et al. "TRMM precipitation radar." *Advances in Space Research* 25.5 (2000): 969-972.
- Fink, A. H., D. G. Vincent, and V. Ermert. "Rainfall types in the West African Sudanian zone during the summer monsoon 2002." *Monthly weather review* 134.8 (2006): 2143-2164.
- Maranan, M., Fink, A. H., and Knippertz, P., 2017: Identification and Climatology of Rainfall Types over Southern West Africa, *Q. J. Royal Meteorol. Soc.*, in preparation
- Flamant, C., C. Lavaysse, M. Todd, J.-P. Chaboureau, and J. Pelon, 2009: Multi-platform observations of a representative springtime case of Bod´el´e and Sudan dust emission, transport and scavenging over West Africa. *Quart. J. Roy. Meteor. Soc.*, 135, 413–430.
- Lafore, J. P., and Coauthors, 1998: The Méso-NH Atmospheric Simulation System. Part I: adiabatic formulation and control simulations. *Annales Geophysicae*, 16 (1), 90–109.
- Reinares Martínez, I. and J.-P. Chaboureau, 2017a: Precipitation and mesoscale convective systems for explicit versus parameterized convection over northern Africa, *Mon. Weather Rev.*, in revision
- Reinares Martínez, I. and J.-P. Chaboureau, 2017b: radiative effect of dust on mesoscale convective systems: a case study over northern Africa, *Mon. Weather Rev.*, in preparation
- Upton, Graham JG. "A correlation–regression method for tracking rainstorms using rain-gauge data." *Journal of Hydrology* 261.1 (2002): 60-73.